Research Square

Preprints are preliminary reports that have not undergone peer review.
They should not be considered conclusive, used to inform clinical practice,
or referenced by the media as validated information.

Cell-Corr: Fast and coding-free quantification of intracellular dynamics in confocal microscopy time series

Alkiviadis Athanasiadis
Aristotle University of Thessaloniki
Veronica Giourieva
Aristotle University of Thessaloniki
Maria Eleni Parmenidou
Aristotle University of Thessaloniki
George Komis
gkomis@bio.auth.gr

Aristotle University of Thessaloniki

Method Article

Keywords: Cell-Corr, bulk analysis, intracellular dynamics, Pearson correlation coefficient

Posted Date: November 23rd, 2026

DOI: https://doi.org/10.21203/rs.3.rs-11727129/v1

License: This work is licensed under a Creative Commons Attribution 4.0 International License.
Read Full License

Additional Declarations: No competing interests reported.

Abstract

The dynamic organization of intracellular components, including cytoskeleton and endoplasmic reticulum (ER) is essential for cell architecture, intracellular trafficking and organelle positioning. Overall temporal dynamics of these components can be analyzed in appropriate time series by virtue of progressive exponential decay of Pearson's correlation coefficient. However, quantifying these dynamics from live-cell fluorescence microscopy time-series, remains challenging, particularly when analysis requires multiple software or programming expertise. Here, Cell-Corr, a standalone, coding-free software for rapid and reproducible quantification of intracellular dynamics is introduced. Cell-Corr integrates image processing, calculation of Pearson's coefficient, statistical analysis, curve fitting and graphical visualization into a streamlined workflow. The software was evaluated using time series of fluorescently labelled actin filaments and ER, under various conditions including the chemical inhibition of actin nucleation and/or bundling with the Arp2/3 inhibitor CK-666 or the formin inhibitor SMIFH2. Comparison with existing analysis tools demonstrated improved processing efficiency and simplified data handling. By integrating established correlation-based approach into an accessible platform, Cell-Corr provides a fast, user-friendly solution for quantitative analysis of intracellular dynamics in live-cell fluorescence microscopy.

Introduction

Actin microfilaments and microtubules are the two core cytoskeletal components of higher plants. Depending on the differentiation stage of a given cell, actin microfilaments exhibit a remarkable diversity of organizational patterns, underlying a wide range of physiological roles within the cell (Zhang et al., 2026). The subcellular occurrence of actin microfilaments is ultimately related with intracellular transport events and organellar positioning during membrane trafficking (Zhang and Staiger, 2021), as evidenced by the rigorous cytoplasmic streaming (Shimmen and Yokota, 2004) and the phototactic or photo-avoiding relocation of chloroplasts in response to differently intense incident light in photosynthetic cell types (Wada and Kong, 2018). Plant actin arrays are also responsible for the interspersing or shaping of widespread structures like the endoplasmic reticulum (Pain et al., 2023; Wang and Hussey, 2015) and the expanding vacuole (Scheuring et al., 2016; Sheahan et al., 2007).

Cortical actin dynamics are driven by a diverse array of actin interacting proteins which regulate actin filament nucleation, crosslinking, severing and end-wise polymerization and depolymerization (Huang et al., 2011), with some mediating interactions of actin filaments with other cellular components including microtubules (Wu et al., 2025). Rigorous research of the molecular mechanisms underlying conditional and developmental actin rearrangements and dynamics has largely relied on the subtractive logic of interfering with the underlying mechanisms. To this end there are many small molecule inhibitors interfering with actin filament integrity *per se*, interacting with monomeric actin or actin filaments and promoting depolymerization (latrunculins, cytochalasins (Foissner and Wasteneys, 2007; Spector et al., 1989)) or stability and polymerization (phalloidins, jasplakinolide;(Holzinger and Blaas, 2016; Pospich et al., 2020)), but there is also an array of drugs that target more specific aspects of actin organization.

Actin nucleation by means of the Arp2/3 complex for example can be inhibited by CK-666 and CK-869 (Hetrick et al., 2013), while actin nucleation and/or bundling can be targeted by SMIFH2 (Small Molecule Inhibitor of Formin Homology 2 domains; (Rizvi et al., 2009)), inhibitors that have been employed in survey of plant actin dynamics in several circumstances (Ali and Kawashima, 2021; Ma et al., 2021; Xu et al., 2024; Zhang et al., 2021).

Owing to their widespread distribution and their global roles in organelle positioning and intracellular transport, actin microfilaments exhibit large-scale dynamic rearrangements over time. Provided that actin filaments are labelled by some appropriate fluorescent marker, such reorganization can be documented by any contemporary means of fluorescence microscopy including conventional confocal laser scanning microscopy, spinning disc microscopy (Ehrhardt and Frommer, 2012) and different modules of super-resolution microscopy including structured illumination and stimulated emission depletion (Komis et al., 2018). Importantly, cortical actin dynamics can be followed by more specialized modalities such as variable angle epifluorescence microscopy (Konopka and Bednarek, 2008). Depending on the acquisition frame rate it is evident that actin dynamics can be documented at the 2 or the 3 space dimensions.

Reports of actin dynamics can be classified on the ground of space and time resolution. The end-wise dynamic behavior of individual actin filaments can be followed by relatively high spatial resolution and acquisition frame rates to report elongation, shrinkage and depolymerization rates, severing frequencies etc. (Henty-Ridilla et al., 2013).

However, actin filaments also exhibit lateral movements and buckling over large scales leading to global dynamics rearrangements of the entire actin cytoskeleton over time. Such rearrangements may accompany diffuse (Bannigan and Baskin, 2005; Takatsuka et al., 2018) or tip cell growth (Ketelaar, 2013; Ketelaar et al., 2003) or can be conditioned by extracellular cues including abiotic inputs (Komis, 2002; Kumar et al., 2023; Lang et al., 2014; Liu et al., 2012; Wang et al., 2011) or biotic interactions (Henty-Ridilla et al., 2013; Leontovyčová et al., 2019; Qin et al., 2021).

To this end, several fluorescent markers that directly label actin filaments have been developed, including plant derived Talin-GFP (Kost et al., 1998) and Fimbrin 1 second Actin Binding Domain-GFP (Sheahan et al., 2004; Wang et al., 2004) and yeast-derived GFP-LifeAct (Smertenko et al., 2010; Vidali et al., 2009), with the latter being considered as the most reliable marker since the first two may produce artefactual actin filament bundling or otherwise altered actin organization owing to overexpression (Ketelaar et al., 2004; Montes-Rodriguez and Kost, 2017).

Quantitative analysis of intracellular dynamics from live-cell microscopy remains challenging, particularly when analysis requires processing of large numbers of time-series datasets. Although several tools are available for image colocalization and correlation analysis, their use can require substantial manual intervention, programming expertise, or sequential processing of individual datasets.

To quantify overall actin dynamicity over time series recordings, the most used method up to date is the pixel intensity correlation method, where the frame-by-frame extend of colocalization is reported, plotting eventually successive values of Pearson's coefficient. This results in exponential decay curves, reflecting the progressive deviation in global actin organization in later frames when superimposed to the first one. This approach has been used routinely in assessments of actin dynamics. Same or similar approaches have been employed to deliver appropriate exponential decay curves (e.g.,(Cvrčková and Oulehlová, 2017)) and such can be easily generated by extrapolating Pearson's indices using colocalization plugins available with ImageJ or Fiji. In examples, where the Pearson's correlation coefficient was used, the preferred tools for colocalization calculations were the corr2 function on MATLAB (Vidali et al., 2010) and fiji plugins (Kočová et al., 2025; Van Gisbergen et al., 2020).

Pairwise correlation coefficients calculated for all possible temporal spacings from a given time-series data have been used to address the role of myosin XI during actin reorganization in *N. benthamiana* leaf epidermal cells (Obara and Tominaga, 2025) based on plotting the corresponding Pearson's coefficients as previously introduced (Vidali et al., 2010) using a built-in MATLAB function "Corr2" (The MathWorks Inc., 2022). This method is not limited to plants as it has been used to study the actomyosin dynamics on animal epithelial cell lines (Klingner et al., 2014). Other studies have used ImageJ or Fiji's plug-ins for pixel intensity correlation method "Coloc2" (Schindelin et al., 2012). However, the built-in functions and the plug-ins lack the bulk analysis option.

In the present study, a coding-free, stand-alone environment for analyzing bulk actin dynamics is provided. Cell-Corr is a user-friendly program designed to analyze multiple datasets of global actin dynamics, integrating statistical tools for comparative studies. Cell-Corr delivered exponential decay experimental and fitted curves from multiple repeats of the same and different experiments and will provide half-time values with statistical significance output. As a proof of concept, Cell-Corr is used herein to compare actin dynamics of *GFP-LifeAct* expressing Arabidopsis hypocotyl epidermal cells in the absence or presence of CK-666 and SMIFH2, two inhibitors of *de novo* actin formation. Moreover, the dynamics of cortical ER in Arabidopsis hypocotyl epidermal cells expressing an *HDEL-GFP* construct is surveyed to show how they are affected by latrunculin B- an actin assembly inhibitor.

Materials and Methods

Plant material and treatments

Arabidopsis thaliana (L) Heynh ecotype Columbia 0 seedlings stably transformed with the *GFP-LifeAct* actin biomarker (Smertenko et al., 2010) and *HDEL-GFP* endoplasmic reticulum marker were used. Seeds were surface sterilized with 30% (v/v) sodium hypochlorite supplemented with 0.02% (v/v) Triton-X100 and allowed to stratify at 4 ^{o}C for 2 days and subsequently left to germinate and grow at long-day conditions (21–22 ^{o}C, 16 h light/ 8 h dark) in a custom-built growth chamber. The seeds were plated on solidified half-strength Murashige-Skoog (Duchefa, Haarlem, the Netherlands) salt medium supplemented with 2% (w/v) sucrose and 1% (w/v) phytoagar (Duchefa, Haarlem, the Netherlands) pH

5.4–5.7. Seeds were grown vertically in Petri dishes. At 4 days after germination (DAG) seedlings were subjected to chemical treatments and microscopy analysis.

For treatments, stock solutions of SMIFH2 (1 mM in DMSO, S4826, Sigma-Aldrich, Darmstadt, Germany), CK-666 (1 mM in DMSO, SML0006, Sigma-Aldrich, Darmstadt, Germany), latrunculin B (1 mM in ethanol, 428020, Sigma-Aldrich, Darmstadt, Germany) were prepared and stored at -20°C. For SMIFH2 treatment seeds were grown in half-strength MS supplemented with 10 μM for 4 DAG and subjected to live imaging. Three to four-day old seedlings were treated for 10 min with 1 μM CK-666 or with 10 nM latrunculin B and live imaging analysis was followed.

Live cell imaging

Time series datasets of hypocotyls epidermal cells of *GFP-LifeAct* and *HDEL-GFP* were acquired with confocal laser scanning microscope (LSM 780, Carl Zeiss, Germany) with Plan-Apochromat 40x/1.3 NA oil immersion objective and equipped with AxioCam MRc 5 (Carl Zeiss, Berlin, Germany). GFP was excited at 488 nm (laser intensity 5%) and detected between 497–519 and 2.22–4.40 airy unit (AU) pinhole. Time series datasets were post-processed to *.avi movies with Zeiss Zen 3.13 (Zen lite, Blue version) software.

Software Development and Implementation

The core operations for colocalization analysis were created using the Tkinter toolkit and it was purposefully made similar to ImageJ's graphical interface. For easy accession to the file system, Cell-Corr uses the tkinter.filedialog method. The image processing of the sample videos, retrieved by confocal microscopy (8-bit stack of images), is achieved using standard Python image analysis libraries, specifically openCV (Bradski, 2000). Mathematical calculations and data handling are performed by NumPy (Harris et al., 2020) and Pandas libraries, while statistical analysis functions are accomplished through the SciPy (Virtanen et al., 2020) package. To be able to provide ready for publishing figures, Matplotlib (Hunter, 2007) library was imported to the script. The whole script was converted into an executable (.exe format) by PyInstaller. The Cell-Corr executable can be installed directly on a windows environment. A GUI version of Cell-Corr for Unix-based operating systems (GNU/Linux and MacOS) is also available and can accessed through Bash shell commands (tested on Ubuntu). Complete guides for installation of the software are provided on the GitHub page:
https://github.com/AlkiviadisAthanasiadis/Cell-Corr

Dynamics analysis is automated and colocalization analysis is achieved by implementing the SciPy library and the scipy.stats.pearsonr() function. For video processing and ROI selection, the .avi files are imported to a tkinter canvas using the library openCV2. For data frame preparation and initial statistics, Cell-Corr contains a built-in option for preparing the data frames before plotting. This function is based on Pandas (McKinney, 2011) python library in order to create data frames. For the depiction of dynamics,

five equally time-spaced frames of a sample video, with different color each was introduced to the software. To produce the color coded-hyper stack the software subtracts the background and adds the pictures in order of decreasing intensity. The final image can be saved as a .png or any other image file format (.eps, .jpeg, .pgf, .pdf, .ps, .bimp, .svg, .tiff, .webp).

Plotting and exponential model fitting

The model fitting is conducted by the scipy.optimize.curve_fit function and t-half value is calculated from the received parameters. The model in use is described by the following formula:

$$y\left(t\right) = a1 * e^{-b1*t} + a2 * e^{-b2*t} + c$$

Statistical analysis

Statistical tests are integrated into the software via SciPy and Statsmodels libraries and include one-way ANOVA and Kruskal-Wallis tests (depending on the normality test). In case of more than two datasets statistical analysis can be combined with post hoc (pairwise comparison with Tukey's test for ANOVA and Dunn's test for Kruskal-Wallis tests). Statistical significance has been set to $p < 0.05$.

Results

Pipeline of Cell-Corr software

In this study, an image and statistical analysis approach was developed to quantify the dynamics of cellular components, including actin filaments and endoplasmic reticulum. To enable this analysis, a computational pipeline was implemented following the steps described (Fig. 1, Fig. 2).

Cell-Corr was designed as a Graphical User Interphase (GUI) and open-source stand-alone program based on python programing language (version 3.13). The core functions, accessible *via* the main menu, allow the user to conduct all the necessary procedures after receiving the time-series (Fig. 1a).

Cellular dynamics are measured as the change of Pearson's Correlation Coefficient (PCC) over time. Cell-Corr uses two individual methods of PCC calculation. The first method (Vidali et al., 2010) measures the PCC between frames of all possible time intervals. The values retrieved by equally time spaced frames get averaged and plotted as an exponential decay as the interval duration increases (Fig. 1b). The second method (Kočová et al., 2025) incorporates a slightly different way to describe intracellular dynamics. Specifically, PCC values are measured for each frame compared to the initial one and plotted as a function of time (Fig. 1b). Both ways are automated and can produce the data needed for each sample video through a button and integrate them into a data frame (Fig. 1a).

Cell-Corr was deliberately designed to support .avi video formats, as they are known to use minimum compression without data loss, despite the large file size (Fig. 2). After importation of .avi the user can

convert the file to 8-bit file format by the Grayscale button, as 8-bit conversion is necessary for obtaining PCC. Next the user can select the ROI by drawing an N-gon shape that gets converted to a mask and subtracts the background (Fig. 2a). The user should save the processed videos in a unique file each as needed for the following analysis (Fig. 2a).

Subsequently, in order to process the analysis of time-frames the user provides the scanning speed used for retrieving the time-series by confocal microscopy. Each study technique for the dynamics analysis is available through the appropriately named button in the module called Colocalization Analysis (Fig. 2b). After conducting the chosen analysis for every sample video prepared, there are additional functions for calculating the mean and standard error for each row (basic colocalization analysis (Kočová et al., 2025) or time interval averaging colocalization analysis (Vidali et al., 2010)). As a final step Cell-Corr provides a normality test to check if the data follows the normal distribution for each individual time interval (Fig. 2b).

Additionally, Cell-Corr integrates the matplotlib library for plotting in a separate module called Plot Analysis (Fig. 2c, d). For reliability reasons the user decides which data sets to use (.csv saved from the colocalization analysis window) and the program provides the curves with the standard error (Fig. 2c). After importing a data set, the software contains a function for estimating a double exponential decay model and calculating the t-half value (Fit Exp Decay button) (Fig. 2c).

For normally distributed data and two or less datasets, Cell-Corr provides an one-way ANOVA test (Run ANOVA button, Fig. 2c). If this parameter is not justified, the user can use the Kruskal-Wallis test (Run Kruskal-Wallis button, Fig. 2c). In the case of more than two data sets, a pairwise comparison among them using Dunn's post hoc test is also implemented (Run Kruskal-Wallis with Post Hoc button or Run ANOVA with Post Hoc button, Fig. 2c). A new window gets created with the post-hoc analysis results (Fig. 2d). Except for the colocalization analysis and the graphical analysis, Cell-Corr provides the user the choice of color-coded hyper-stack (Image◊color coded hyper-stack button, Fig. 2e).

To summarize, Cell-Corr is a standalone software that provides a user-friendly environment for colocalization analysis, a range of statistical analysis tools and graphical visualization of time-series datasets without requiring any programming skills.

Comparison of methods for evaluating cortical ER dynamics

To estimate the capabilities of Cell-Corr, ER labeled samples of the stably expressing *HDEL-GFP* line were analyzed under control conditions and 10 nM latrunculin-B (Lat-B) treatment for 10 min prior to observation (Fig. 3a). The time-series obtained by confocal laser scanning microscope (CLSM) were processed with Cell-Corr, to select the regions-of-interest (ROIs) and each dataset was analyzed using both methods described (Fig. 3b,c; see also Movie 1 and Movie 2). The graphical outcome of the prior analysis indicates a slight decrease in the ER dynamic behavior on the Lat-B treated seedlings (at t = 57 s $PCC_{control}$ = 0.67 ± 0.024 vs PCC_{LatB}= 0.73 ± 0.016 p = 0.0334) which is in accordance with previous

studies (Sparkes et al., 2010). The comparison between the two analytical approaches, time-interval averaged colocalization and colocalization of frames with the initial one, produce almost identical results as shown in the PCC over time graph (Fig. 3b). In addition, the mean PCC values obtained by both samples and techniques and the normality test *p*-value in four different timepoints are also compared (Table 1).

Table 1
Correlation Coefficients of HDEL-GFP ER marker as a function of time intervals using (alternative method) or not (Vidali's method) identical interval averaging.

	Correlation/Normality *p* value			
	14 s	**28 s**	**43 s**	**57 s**
HDEL alternative method	0.7967/0.2480	0.7317/0.1551	0.6939/0.1458	0.6763/0.0603
HDEL Vidali's method	0.7929/0.0657	0.7307/0.0349	0.6947/0.0453	0.6763/0.0603
HDEL + LatB alternative method	0.8567/0.3401	0.7977/0.4883	0.7541/0.9317	0.7315/0.9049
HDEL + LatB Vidali's method	0.8489/0.7711	0.7907/0.8079	0.7566/0.9443	0.7315/0.9049

Another internal function of Cell-Corr, model fitting and t1/2 value calculation, was also tested using the same samples. When estimating the software's capability to calculate the half time value, the values compared to the values calculated for each individual time-series using the same model -statistical significance was evaluated by t-test. The mean t1/2 values from the separated samples were calculated, giving a mean of 14.25 ± 2.44 s for the ER sample with correlation to the initial frame, 10.91 ± 2.07 s with time-interval averaging, 19.95 ± 2.71 s for the LatB treatment with correlation to the initial frame and 14.54 ± 1.85 s with time-interval averaging. Cell-Corr's estimated t1/2 values were 9.01 s *vs* 15.64 s, 8.91 s *vs* 13.1 s for control *vs* LatB treated samples, respectively (Fig. 3c). It was shown that the time-interval averaged correlation had comparable half time value to the one calculated based on the correlation to initial time frame (Fig. 3c).

Cell-Corr enables efficient and reproducible analysis of intracellular dynamics

To further evaluate the performance and applicability of Cell-Corr, its analysis capabilities were compared with currently available tools for colocalization and time series analysis. The comparison was focused on the type of analysis produced (PCC, Manders etc), its ease of use, speed and the range of quantitative metrics (Table 2). Cell-Corr was compared to representative currently available tools including a ImageJ's plugin JaCoP (Bolte and Cordelières, 2006), a Fiji's plugin Coloc2 (Schindelin et al., 2012) and a MATLAB built-in function Corr2 (The MathWorks Inc., 2022). Cell-Corr showed more advantages compared to the other tools as it did not require any programming skills in comparison to Corr2, it provided automated and bulked datasets analysis which made the video post-processing much

faster and convenient (approximately 1 video per 1 min which was at least 3-times faster compared to the other available tools) (Table 2).

Table 2
Comparison of Cell-Corr to ImageJ plugin JaCoP, Coloc2 and Corr2.

Type	**Cell-Corr**	**JaCoP**	**Coloc2**	**Corr2**
	Standalone software	**ImageJ plug-in**	**Fiji plug-in**	**Built-in function**
Analysis	Pearson	Pearson Manders, k1 and k2, overlap, Costes, Li	Pearson Manders, Costes, Li	Pearson
Requirement for programming skills	No	No	No	Yes (MATLAB)
Automation	Yes	No	No	No
Analysis integration	Yes	No	No	No
Analysis speed	1 video/1min	1 video/3-5min	1 video/3-5min	> 1 video/3-5min
Statistical analysis	Yes	Yes	Yes	No
Plot data	Yes	No	No	No
Exponential model estimation	Yes	No	No	No
t-half value calculation	Yes	No	No	No

Analysis speed refers to videos of 20 frames. Time includes post-processing (masking etc). Analysis integration, statistical analysis, plot data, exponential model estimation and t-half calculation refers to analysis for generation of final data for visualization of structures analysis.

Subsequently, JaCoP was selected as representative tool currently available solution and analyzed the same dataset as Cell-Corr (Fig. 4). For the analysis control 4-day-old hypocotyl epidermal cells from stably expressing *GFP-LifeAct* line were selected (a representative time series is presented in Fig. 4A, Movie 3) and further analyzed. Cell-Corr produced comparable quantitative measurements while requiring fewer user-intervention.

Figure 4 Comparison of PCCs between Cell-Corr and ImageJ plug-in JaCoP analysis. (a) Representative timeframes and color-coded hyper-stack of 4-day-old seedlings of hypocotyl epidermal cells of stable lines expressing *GFP-LifeAct*. (b) Quantification of actin dynamics with PCCs using Cell-Corr has no significant difference from the ones calculated with JaCoP (12.52s: $p = 0.85$, 34.43s: $p = 0.862$, 43.82s: $p = 0.839$ and 56.34s: $p = 0.931$ as tested with Kruskal-Wallis). (c) Distribution of ROIs Correlation

Coefficients among the initial and final frames as depicted in panel b. In total 30 cells were analyzed (from at least 10 seedlings). Not significant: ns. Scale bar: 20 μm.

The correlation coefficients had no statistically significant differences between Cell-Corr and JaCoP as presented by the fitted exponential decay (Fig. 4B) and the data distribution of ROIs depicted in Fig. 4C. The half-life was determined with Cell-Corr smaller compared to the one calculated from PCCs of JaCoP (compare t1/2 Cell-Corr 31.97 s to t1/2 JaCoP 33.08 s) without any statistical significance. To summarize, Cell-Corr is more convenient, reliable, user friendly and much faster providing complete dynamics and graphical analysis compared to available tools.

F-Actin Dynamics depiction under the treatment of the nucleator inhibitors SMIFH2 and CK-666

To further evaluate the applicability of Cell-Corr to reliable and fast intracellular dynamics analysis, the software was used to analyze datasets from two treatments with SMIFH2 and CK-666 on *GFP-LifeAct* transgenic seedlings and the outcome was compared and plotted with control samples (Fig. 5a). Both SMIFH2 and CK-666 are known for inhibiting the formin nucleator family and the ARP2/3 complex, respectively, which are used for actin nucleation in eukaryotic cells (Hetrick et al., 2013). For this analysis colocalization to initial frame was used to evaluate dynamics. As the PCC over time diagram indicates both inhibitors significantly increased the dynamic behavior of F-Actin microfilaments (p-value < 0.0001 for both CK-666 and SMIFH2 treatments, Kruskal- Wallis test and Dunn's post hoc at four equally spaced time points (Fig. 5b; see also Movie 4, Movie 5 and Movie 6). The t-half value of each dataset was also calculated as quantification factor (control: t1/2 = 17.36 s *vs* CK-666: t1/2 = 22.28 s and SMIFH2: t1/2 = 13.88, Fig. 5b). Treatment with CK-666 lead to slower *GFP-LifeAct* decay, practically meaning higher residence time and increased persistence of *GFP-LifeAct* spatial pattern while treatment with SMIFH2 decreased the molecule's stability compared to control (Fig. 5b). As a last optical representation of the data violin plots of the comparisons between the last and first frame per video of every sample are compared -showing the additional statistically significant decrease in correlation coefficients in inhibitors treatments compared to control (Fig. 5c).

Discussion

Here, the standalone software, Cell-Corr, was developed for the bulk analysis of dynamics of cellular compartments inadequate of any programming skills. Cell-Corr integrates temporal PCC analysis, exponential-decay fitting, visual and batch processing into an accessible, code-free workflow including graphical visualization. It can process more than 50 videos in less than an hour with reasonable sized GPU, less than 2 GB storage and is operatable in Windows, MacOS and Linux operating systems (Table S1). The software and representative datasets are open-source allowing researchers to use, to further process and adjust to their specific needs. The analysis of PCC is automated and efficient and reproducible analysis of intracellular compartments with low deviation comparing the basic colocalization analysis (Vidali et al., 2010) and time-interval averaged colocalization (Kočová et al.,

2025). The ability to automatically perform these calculations across multiple time-series datasets represents an important practical advantage.

A major advantage of Cell-Corr compared with existing approaches is the integration of bulk analysis and visualization within a single workflow. Conventional image-analysis pipelines frequently require the user to move between microscopy software, image-analysis plugins, spreadsheets and statistical packages. This fragmented workflow can become inefficient when multiple time-series datasets need to be analyzed. In contrast, Cell-Corr allows processed datasets to be analyzed and exported in a consistent format, while the plotting module provides direct visualization of correlation decay, fitted curves and data distributions.

Processing speed is another relevant advantage. The ability to analyze approximately one video per minute represents a substantial reduction in analysis time compared with the workflows evaluated here. This becomes increasingly important as live-cell microscopy experiments generate larger datasets and biological studies require analysis of many independent cells, conditions and time points.

The agreement between t1/2 values calculated using Cell-Corr and those obtained independently from the same datasets supports the reliability of the implemented fitting procedure. Similarly, the close agreement between Cell-Corr and JaCoP for both PCC values and t1/2 demonstrates that the software can reproduce measurements obtained using an established correlation-based analysis workflow. The ER analysis similarly illustrates the potential of Cell-Corr to quantify relatively subtle changes in intracellular dynamics. The ability to detect such changes highlights the potential applicability of the approach beyond actin and suggests that Cell-Corr may be useful for analyzing other dynamic membrane or cytoplasmic compartments.

Statistical analysis should be selected according to the experimental design rather than simply according to the availability of a statistical test within the software. In particular, time-series measurements from the same cell or video are not necessarily independent observations, and multiple time points may require approaches that account for repeated measurements. Cell-Corr's integrated statistical functions are therefore intended to facilitate exploratory and routine analysis, while more complex experimental designs may require dedicated statistical software or mixed-effects modelling.

Overall, Cell-Corr provides a streamlined approach for converting live-cell microscopy time-series into quantitative measurements of intracellular dynamics. Validation against established correlation-based analysis demonstrates comparable PCC and decay measurements, while automated processing substantially reduces the time and manual intervention required for analysis. The application to ER and actin dynamics further demonstrates that the approach can detect biologically relevant changes in dynamic cellular structures. The main contribution of Cell-Corr is therefore not the introduction of a new correlation metric, but the integration and automation of established quantitative approaches into an accessible workflow for time-series microscopy. This makes the analysis more practical for routine use and facilitates the processing of larger datasets. Future development could extend Cell-Corr to additional image formats (so far only .avi files can be analyzed), multidimensional datasets, additional

colocalization coefficients (such as Manders overlap coefficients), automated ROI detection (when used in appropriately labeled samples), and more sophisticated statistical models for repeated-measures time-series data. Such extensions could broaden its applicability to diverse live-cell imaging experiments and further reduce the barrier between acquisition of microscopy datasets and quantitative analysis.

Abbreviations

ANOVA
Analysis of variance
AU
airy unit
CLSM
confocal laser scanning microscope
DAG
days after germination
ER
endoplasmic reticulum
GUI
Graphical User Interphase
LatB
latrunculin B
PCC
Pearson’s Correlation Coefficient
K-W
Kruskal-Wallis
ROI
region of interest
SMIFH2
Small Molecule Inhibitor of Formin Homology 2 domain

Declarations

Competing interests.

The authors declare any competing or financial interests.

Data and resource availability

The Cell-Corr software, the code, user instructions and troubleshooting are available and can be freely downloaded from the GitHub repository (github.com/AlkiviadisAthanasiadis/Cell-Corr).

Funding

VG is supported by the Hellenic Foundation for Research and Innovation (HFRI) under the 4th Call for HFRI PhD Fellowships (11007). GK was supported by funds from the Special Research Account (ELKE) of AUTH.

Author Contribution

AA wrote the Cell Corr code, VG contributed transgenic plants, time lapsed series of actin dynamics and quantitative analysis with appropriate Image J plugins together with AA, MEP contributed imaging of actin dynamics and GK contributed concept, funding, infrastructure, data analysis and manuscript drafting together with AA and VG. All authors reviewed and approved the manuscript.

Acknowledgement

We would like to thank Assoc. Prof. Andrei Smertenko (Institute of Biological Chemistry, Washington State University, Pullman, WA, USA) and Assist Prof. Joseph McKenna (School of Life Sciences, University of Warwick, Coventry CV4 7AL, United Kingdom) for kindly providing the seed stock GFP-LifeAct and HDEL-GFP, respectively. We thank Dr. Stylianos Poulios for critical reading of the manuscript.

Data Availability

The Cell-Corr software, the code, user instructions and troubleshooting are available and can be freely downloaded from the GitHub repository (github.com/AlkiviadisAthanasiadis/Cell-Corr).

References

1. Ali MF, Kawashima T (2021) Formins control dynamics of F-actin in the central cell of *Arabidopsis thaliana*. Plant Signal Behav 16:1920192. https://doi.org/10.1080/15592324.2021.1920192
2. Bannigan A, Baskin TI (2005) Directional cell expansion — turning toward actin. Curr Opin Plant Biol 8:619–624. https://doi.org/10.1016/j.pbi.2005.09.002
3. Bolte S, Cordelières FP (2006) A guided tour into subcellular colocalization analysis in light microscopy. J Microsc 224:213–232. https://doi.org/10.1111/j.1365-2818.2006.01706.x
4. Bradski G (2000) The OpenCV Library. Dr Dobb's J Softw Tools 120:122–125
5. Cvrčková F, Oulehlová D (2017) A new kymogram-based method reveals unexpected effects of marker protein expression and spatial anisotropy of cytoskeletal dynamics in plant cell cortex. Plant Methods 13:19. https://doi.org/10.1186/s13007-017-0171-9

6. Ehrhardt DW, Frommer WB (2012) New Technologies for 21st Century Plant Science. Plant Cell 24:374–394. https://doi.org/10.1105/tpc.111.093302
7. Foissner I, Wasteneys GO (2007) Wide-Ranging Effects of Eight Cytochalasins and Latrunculin A and B on Intracellular Motility and Actin Filament Reorganization in Characean Internodal Cells. Plant Cell Physiol 48:585–597. https://doi.org/10.1093/pcp/pcm030
8. Harris CR, Millman KJ, Van Der Walt SJ, Gommers R, Virtanen P, Cournapeau D, Wieser E, Taylor J, Berg S, Smith NJ, Kern R, Picus M, Hoyer S, Van Kerkwijk MH, Brett M, Haldane A, Del Río JF, Wiebe M, Peterson P, Gérard-Marchant P, Sheppard K, Reddy T, Weckesser W, Abbasi H, Gohlke C, Oliphant TE (2020) Array programming with NumPy. Nature 585:357–362. https://doi.org/10.1038/s41586-020-2649-2
9. Henty-Ridilla JL, Li J, Blanchoin L, Staiger CJ (2013) Actin dynamics in the cortical array of plant cells. Curr Opin Plant Biol 16:678–687. https://doi.org/10.1016/j.pbi.2013.10.012
10. Henty-Ridilla JL, Shimono M, Li J, Chang JH, Day B, Staiger CJ (2013) The Plant Actin Cytoskeleton Responds to Signals from Microbe-Associated Molecular Patterns. PLoS Pathog 9:e1003290. https://doi.org/10.1371/journal.ppat.1003290
11. Hetrick B, Han MS, Helgeson LA, Nolen BJ (2013) Small Molecules CK-666 and CK-869 Inhibit Actin-Related Protein 2/3 Complex by Blocking an Activating Conformational Change. Chem Biol 20:701–712. https://doi.org/10.1016/j.chembiol.2013.03.019
12. Holzinger A, Blaas K (2016) Actin-Dynamics in Plant Cells: The Function of Actin-Perturbing Substances: Jasplakinolide, Chondramides, Phalloidin, Cytochalasins, and Latrunculins. In: Gavin RH (ed) Cytoskeleton Methods and Protocols, Methods in Molecular Biology. Springer New York, New York, NY, pp 243–261. https://doi.org/10.1007/978-1-4939-3124-8_13
13. Huang S, Xiang Y, Ren H (2011) Actin-Binding Proteins and Actin Dynamics in Plant Cells. In: Liu B (ed) The Plant Cytoskeleton, Advances in Plant Biology. Springer New York, New York, NY, pp 57–80. https://doi.org/10.1007/978-1-4419-0987-9_3
14. Hunter J, Matplotlib (2007) A 2D Graphics Environment. Comput Sci Eng 9, 90–95
15. Ketelaar T (2013) The actin cytoskeleton in root hairs: all is fine at the tip. Curr Opin Plant Biol 16:749–756. https://doi.org/10.1016/j.pbi.2013.10.003
16. Ketelaar T, Anthony RG, Hussey PJ (2004) Green Fluorescent Protein-mTalin Causes Defects in Actin Organization and Cell Expansion in Arabidopsis and Inhibits Actin Depolymerizing Factor's Actin Depolymerizing Activity in Vitro. Plant Physiol 136:3990–3998. https://doi.org/10.1104/pp.104.050799
17. Ketelaar T, De Ruijter NCA, Emons AMC (2003) Unstable F-Actin Specifies the Area and Microtubule Direction of Cell Expansion in Arabidopsis Root Hairs. Plant Cell 15:285–292. https://doi.org/10.1105/tpc.007039
18. Klingner C, Cherian AV, Fels J, Diesinger PM, Aufschnaiter R, Maghelli N, Keil T, Beck G, Tolić-Nørrelykke IM, Bathe M, Wedlich-Soldner R (2014) Isotropic actomyosin dynamics promote

organization of the apical cell cortex in epithelial cells. J Cell Biol 207:107–121. https://doi.org/10.1083/jcb.201402037

19. Kočová H, Žárský V, Cvrčková F (2025) The fate and function of the Arabidopsis Class I formin AtFH1 during central vacuole biogenesis in the rhizodermis. Front Plant Sci 16:1685260. https://doi.org/10.3389/fpls.2025.1685260
20. Komis G (2002) Hyperosmotic stress-induced actin filament reorganization in leaf cells of Chlorophyton comosum. J Exp Bot 53:1699–1710. https://doi.org/10.1093/jxb/erf018
21. Komis G, Novák D, Ovečka M, Šamajová O, Šamaj J (2018) Advances in Imaging Plant Cell Dynamics. Plant Physiol 176:80–93. https://doi.org/10.1104/pp.17.00962
22. Konopka CA, Bednarek SY (2008) Variable-angle epifluorescence microscopy: a new way to look at protein dynamics in the plant cell cortex. Plant J 53:186–196. https://doi.org/10.1111/j.1365-313X.2007.03306.x
23. Kost B, Spielhofer P, Chua N (1998) A GFP-mouse talin fusion protein labels plant actin filaments *in vivo* and visualizes the actin cytoskeleton in growing pollen tubes. Plant J 16:393–401. https://doi.org/10.1046/j.1365-313x.1998.00304.x
24. Kumar S, Jeevaraj T, Yunus MH, Chakraborty S, Chakraborty N (2023) The plant cytoskeleton takes center stage in abiotic stress responses and resilience. Plant Cell Environ 46:5–22. https://doi.org/10.1111/pce.14450
25. Lang I, Sassmann S, Schmidt B, Komis G (2014) Plasmolysis: Loss of Turgor and Beyond. Plants 3:583–593. https://doi.org/10.3390/plants3040583
26. Leontovyčová H, Kalachova T, Trdá L, Pospíchalová R, Lamparová L, Dobrev PI, Malínská K, Burketová L, Valentová O, Janda M (2019) Actin depolymerization is able to increase plant resistance against pathogens via activation of salicylic acid signalling pathway. Sci Rep 9:10397. https://doi.org/10.1038/s41598-019-46465-5
27. Liu SG, Zhu DZ, Chen GH, Gao X-Q, Zhang XS (2012) Disrupted actin dynamics trigger an increment in the reactive oxygen species levels in the Arabidopsis root under salt stress. Plant Cell Rep 31:1219–1226. https://doi.org/10.1007/s00299-012-1242-z
28. Ma Z, Liu X, Nath S, Sun H, Tran TM, Yang L, Mayor S, Miao Y (2021) Formin nanoclustering-mediated actin assembly during plant flagellin and DSF signaling. Cell Rep 34:108884. https://doi.org/10.1016/j.celrep.2021.108884
29. McKinney W (2011) Pandas: A Foundational Python Library for Data Analysis and Statistics. Python High Perform Sci Comput 14:1–9
30. Montes-Rodriguez A, Kost B (2017) Direct Comparison of the Performance of Commonly Employed In Vivo F-actin Markers (Lifeact-YFP, YFP-mTn and YFP-FABD2) in Tobacco Pollen Tubes. Front. Plant Sci. 8, 1349. https://doi.org/10.3389/fpls.2017.01349
31. Obara J, Tominaga M (2025) Dynamics of full-length Arabidopsis myosin XI and its involvement in actin remodeling. Plant Cell Physiol 66:1454–1467. https://doi.org/10.1093/pcp/pcaf097

32. Pain C, Tolmie F, Wojcik S, Wang P, Kriechbaumer V (2023) intER-ACTINg: The structure and dynamics of ER and actin are interlinked. J Microsc 291:105–118. https://doi.org/10.1111/jmi.13139
33. Pospich S, Merino F, Raunser S (2020) Structural Effects and Functional Implications of Phalloidin and Jasplakinolide Binding to Actin Filaments. Structure 28:437–449e5. https://doi.org/10.1016/j.str.2020.01.014
34. Qin L, Liu L, Tu J, Yang G, Wang S, Quilichini TD, Gao P, Wang H, Peng G, Blancaflor EB, Datla R, Xiang D, Wilson KE, Wei Y (2021) The ARP2/3 complex, acting cooperatively with Class I formins, modulates penetration resistance in Arabidopsis against powdery mildew invasion. Plant Cell 33:3151–3175. https://doi.org/10.1093/plcell/koab170
35. Rizvi SA, Neidt EM, Cui J, Feiger Z, Skau CT, Gardel ML, Kozmin SA, Kovar DR (2009) Identification and Characterization of a Small Molecule Inhibitor of Formin-Mediated Actin Assembly. Chem Biol 16:1158–1168. https://doi.org/10.1016/j.chembiol.2009.10.006
36. Scheuring D, Löfke C, Krüger F, Kittelmann M, Eisa A, Hughes L, Smith RS, Hawes C, Schumacher K, Kleine-Vehn J (2016) Actin-dependent vacuolar occupancy of the cell determines auxin-induced growth repression. Proc. Natl. Acad. Sci. U.S.A. 113, 452–457. https://doi.org/10.1073/pnas.1517445113
37. Schindelin J, Arganda-Carreras I, Frise E, Kaynig V, Longair M, Pietzsch T, Preibisch S, Rueden C, Saalfeld S, Schmid B, Tinevez J-Y, White DJ, Hartenstein V, Eliceiri K, Tomancak P, Cardona A (2012) Fiji: an open-source platform for biological-image analysis. Nat Methods 9:676–682. https://doi.org/10.1038/nmeth.2019
38. Sheahan MB, Rose RJ, McCurdy DW (2007) Actin-filament-dependent remodeling of the vacuole in cultured mesophyll protoplasts. Protoplasma 230:141–152. https://doi.org/10.1007/s00709-006-0236-5
39. Sheahan MB, Staiger CJ, Rose RJ, McCurdy DW (2004) A Green Fluorescent Protein Fusion to Actin-Binding Domain 2 of Arabidopsis Fimbrin Highlights New Features of a Dynamic Actin Cytoskeleton in Live Plant Cells. Plant Physiol 136:3968–3978. https://doi.org/10.1104/pp.104.049411
40. Shimmen T, Yokota E (2004) Cytoplasmic streaming in plants. Curr Opin Cell Biol 16:68–72. https://doi.org/10.1016/j.ceb.2003.11.009
41. Smertenko AP, Deeks MJ, Hussey PJ (2010) Strategies of actin reorganisation in plant cells. J Cell Sci 123:3019–3028. https://doi.org/10.1242/jcs.071126
42. Sparkes I, Runions J, Hawes C, Griffing L (2010) Movement and Remodeling of the Endoplasmic Reticulum in Nondividing Cells of Tobacco Leaves. Plant Cell 21:3937–3949. https://doi.org/10.1105/tpc.109.072249
43. Spector I, Shochet NR, Blasberger D, Kashman Y (1989) Latrunculins—novel marine macrolides that disrupt microfilament organization and affect cell growth: I. Comparison with cytochalasin D. Cell Motil. Cytoskeleton 13:127–144. https://doi.org/10.1002/cm.970130302

44. Takatsuka H, Higaki T, Umeda M (2018) Actin Reorganization Triggers Rapid Cell Elongation in Roots. Plant Physiol 178:1130–1141. https://doi.org/10.1104/pp.18.00557
45. The MathWorks Inc (2022) MATLAB version: 9.13.0 (R2022b)
46. Van Gisbergen P, Wu S-Z, Cheng X, Pattavina KA, Bezanilla M (2020) *vivo* analysis of formin dynamics in the moss *P. patens* reveals functional class diversification. J Cell Sci 133:jcs233791. https://doi.org/10.1242/jcs.233791
47. Vidali L, Burkart GM, Augustine RC, Kerdavid E, Tüzel E, Bezanilla M (2010) Myosin XI Is Essential for Tip Growth in *Physcomitrella patens*. Plant Cell 22:1868–1882. https://doi.org/10.1105/tpc.109.073288
48. Vidali L, Rounds CM, Hepler PK, Bezanilla M (2009) Lifeact-mEGFP Reveals a Dynamic Apical F-Actin Network in Tip Growing Plant Cells. PLoS ONE 4:e5744. https://doi.org/10.1371/journal.pone.0005744
49. Virtanen P, Gommers R, Oliphant TE, Haberland M, Reddy T, Cournapeau D, Burovski E, Peterson P, Weckesser W, Bright J, Van Der Walt SJ, Brett M, Wilson J, Millman KJ, Mayorov N, Nelson ARJ, Jones E, Kern R, Larson E, Carey CJ, Polat İ, Feng Y, Moore EW, VanderPlas J, Laxalde D, Perktold J, Cimrman R, Henriksen I, Quintero EA, Harris CR, Archibald AM, Ribeiro AH, Pedregosa F, Van Mulbregt P, SciPy 1.0 Contributors, Vijaykumar, Bardelli A, Rothberg AP, Hilboll A, Kloeckner A, Scopatz A, Lee A, Rokem A, Woods A, Fulton CN, Masson C, Häggström C, Fitzgerald C, Nicholson C, Hagen DA, Pasechnik DR, Olivetti DV, Martin E, Wieser E, Silva E, Lenders F, Wilhelm F, Young F, Price G, Ingold GA, Allen G-L, Lee GE, Audren GR, Probst H, Dietrich I, Silterra JP, Webber J, Slavič JT, Nothman J, Buchner J, Kulick J, Schönberger J, De Miranda Cardoso JL, Reimer JV, Harrington J, Rodríguez J, Nunez-Iglesias JLC, Kuczynski J, Tritz J, Thoma K, Newville M, Kümmerer M, Bolingbroke M, Tartre M, Pak M, Smith M, Nowaczyk NJ, Shebanov N, Pavlyk N, Brodtkorb O, Lee PA, McGibbon P, Feldbauer RT, Lewis R, Tygier S, Sievert S, Vigna S, Peterson S, More S, Pudlik S, Oshima T, Pingel T, Robitaille TJ, Spura TP, Jones T, Cera TR, Leslie T, Zito T, Krauss T (2020) T., Upadhyay, U., Halchenko, Y.O., Vázquez-Baeza, Y., SciPy 1.0: fundamental algorithms for scientific computing in Python. Nat Methods 17, 261–272. https://doi.org/10.1038/s41592-019-0686-2
50. Wada M, Kong S-G (2018) Actin-mediated movement of chloroplasts. J Cell Sci 131:jcs210310. https://doi.org/10.1242/jcs.210310
51. Wang C, Zhang L-J, Huang R-D (2011) Cytoskeleton and plant salt stress tolerance. Plant Signal Behav 6:29–31. https://doi.org/10.4161/psb.6.1.14202
52. Wang P, Hussey PJ (2015) Interactions between plant endomembrane systems and the actin cytoskeleton. Front. Plant Sci 6. https://doi.org/10.3389/fpls.2015.00422
53. Wang Y, Motes CM, Mohamalawari DR, Blancaflor EB (2004) Green fluorescent protein fusions to *Arabidopsis* fimbrin 1 for spatio-temporal imaging of F-actin dynamics in roots. Cell Motil Cytoskeleton 59:79–93. https://doi.org/10.1002/cm.20024
54. Wu Z, Gao L, Ashraf MA, Nan Q (2025) Interaction Between Actin and Microtubules During Plant Development. Cytoskeleton cm.22029 https://doi.org/10.1002/cm.22029

55. Xu L, Cao L, Li J, Staiger CJ (2024) Cooperative actin filament nucleation by the Arp2/3 complex and formins maintains the homeostatic cortical array in *Arabidopsis* epidermal cells. Plant Cell 36:764–789. https://doi.org/10.1093/plcell/koad301
56. Zhang L, Smertenko T, Fahy D, Koteyeva N, Moroz N, Kuchařová A, Novák D, Manoilov E, Smertenko P, Galva C, Šamaj J, Kostyukova AS, Sedbrook JC, Smertenko A (2021) Analysis of formin functions during cytokinesis using specific inhibitor SMIFH2. Plant Physiol 186:945–963. https://doi.org/10.1093/plphys/kiab085
57. Zhang W, Staiger CJ (2021) Revising the Role of Cortical Cytoskeleton during Secretion: Actin and Myosin XI Function in Vesicle Tethering. IJMS 23, 317. https://doi.org/10.3390/ijms23010317
58. Zhang Y, Li J, Xiang Y, Wang P, Le J, Jing Y, Wang T, Wang X, Zhu L, Qian D, Wang G, Liu P, Du F, Kong Z, Fu Y, Guo Y, Huang S, Mao T, Ren H (2026) Cytoskeletal control of development and environmental adaptation in plants. Sci China Life Sci 69:722–767. https://doi.org/10.1007/s11427-024-3067-y

Figures

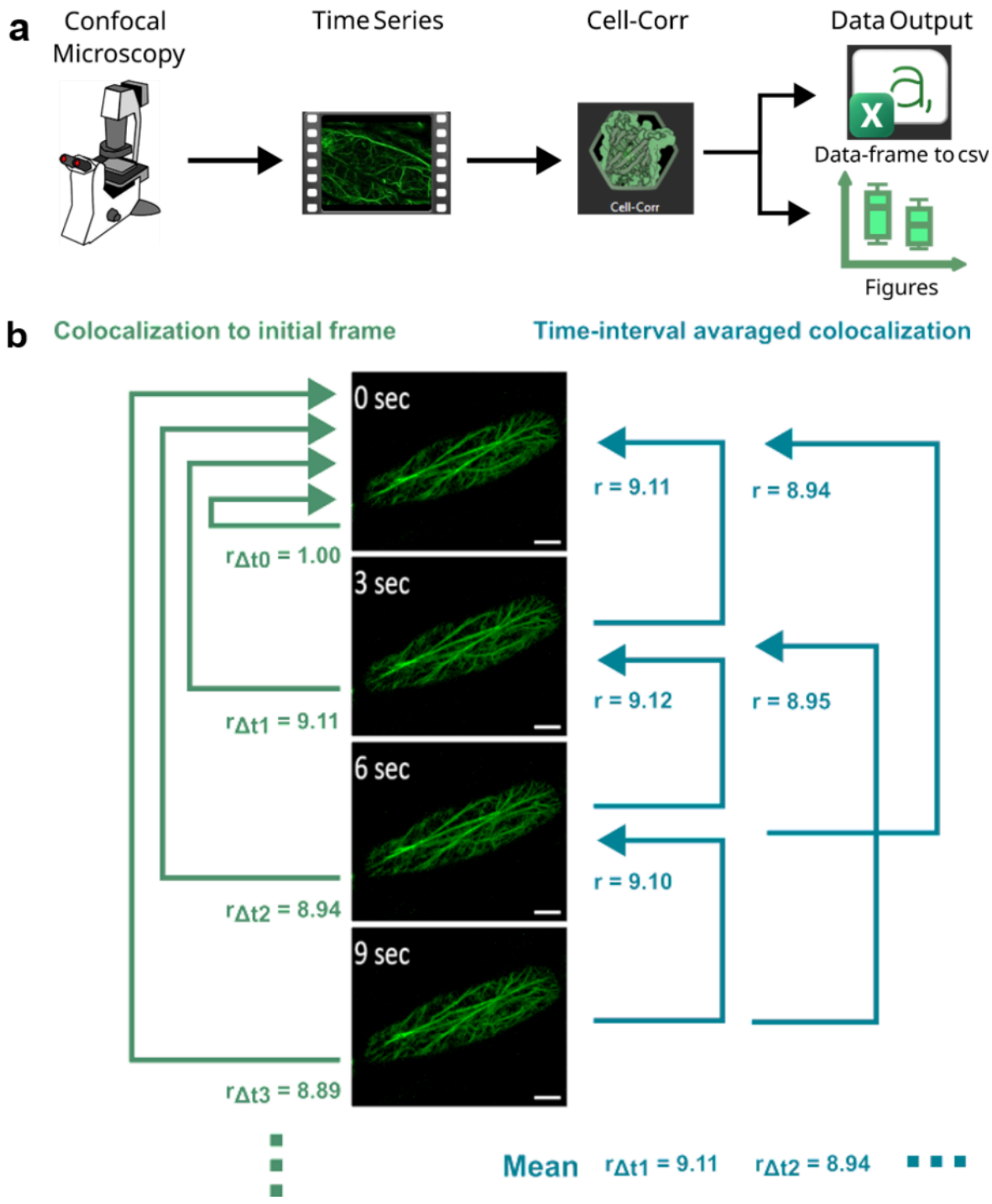

Figure 1

The Pipeline of the intracellular dynamics analysis with Cell-Corr and overview of the integrated techniques. (a) A scheme of the typical procedure regarding the study of descriptive dynamics of intracellular components using Cell-Corr. From microscopy time-series into publishable figures. (b) The principles of the techniques described for evaluating the dynamics of cell components using PCC and comparison between them; On the left side (first technique) dynamical behavior is estimated by

comparison of all consecutive frames to the initial one where on the right side (second technique) dynamicity estimated by averaging the PCC calculated for frames distanced by the same time-interval.

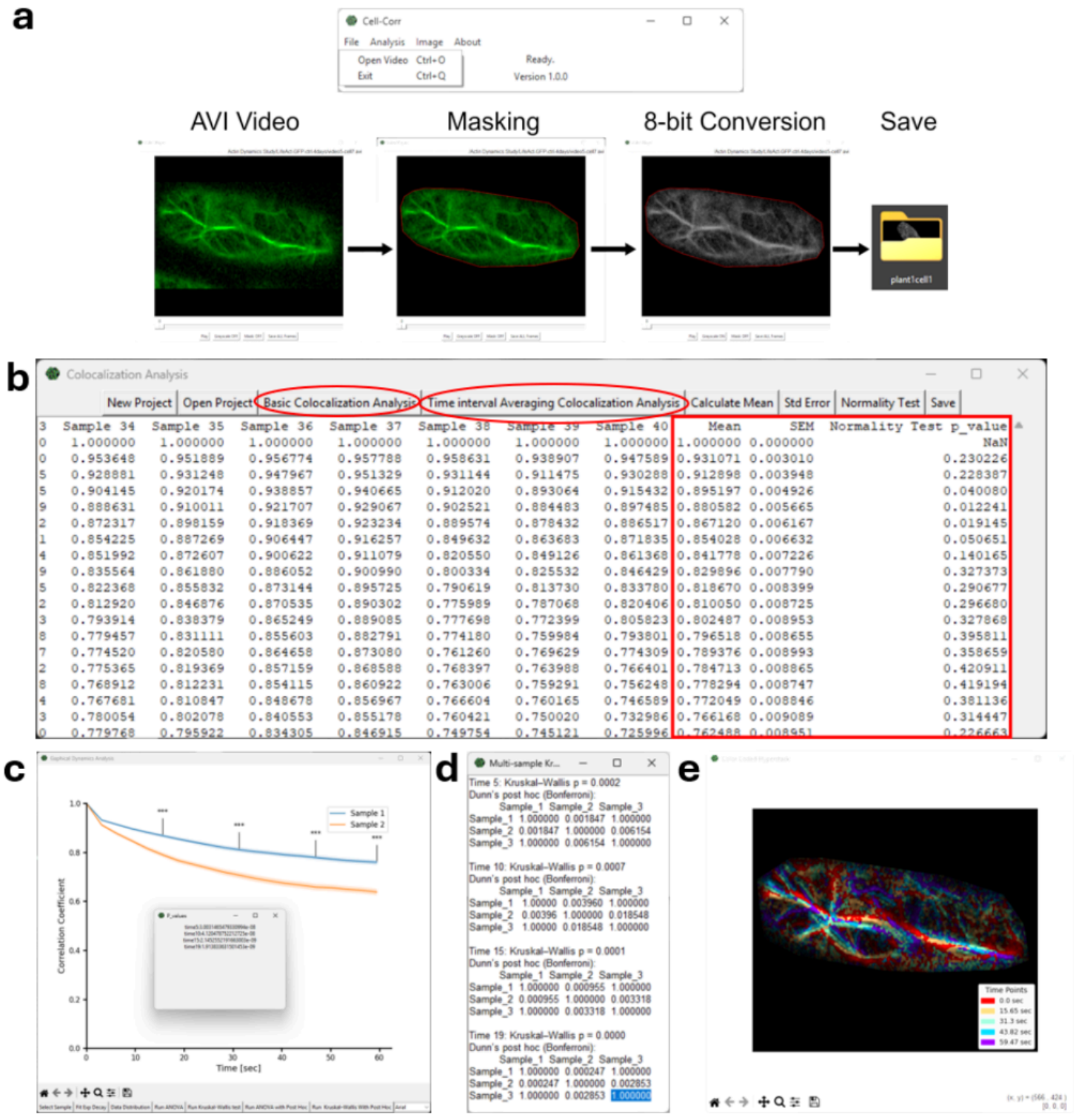

Figure 2

Cell-Corr's GUI overview and functional modules regarding the computational analysis. (a) Video processing module: ROI selection and time-series preparation for colocalization and analysis of

dynamics. (b) Colocalization Analysis module: dataset preparation, automatic PCC calculation and initial statistics. (c) Graphical Analysis module: Dataset plotting, model fitting and statistical comparisons of different datasets. (d) Post hoc result window: evaluation of statistical difference between multiple datasets. (E) Color Coded Hyper-stack: A visual description of overall dynamics by visualizing separate time points with different color.

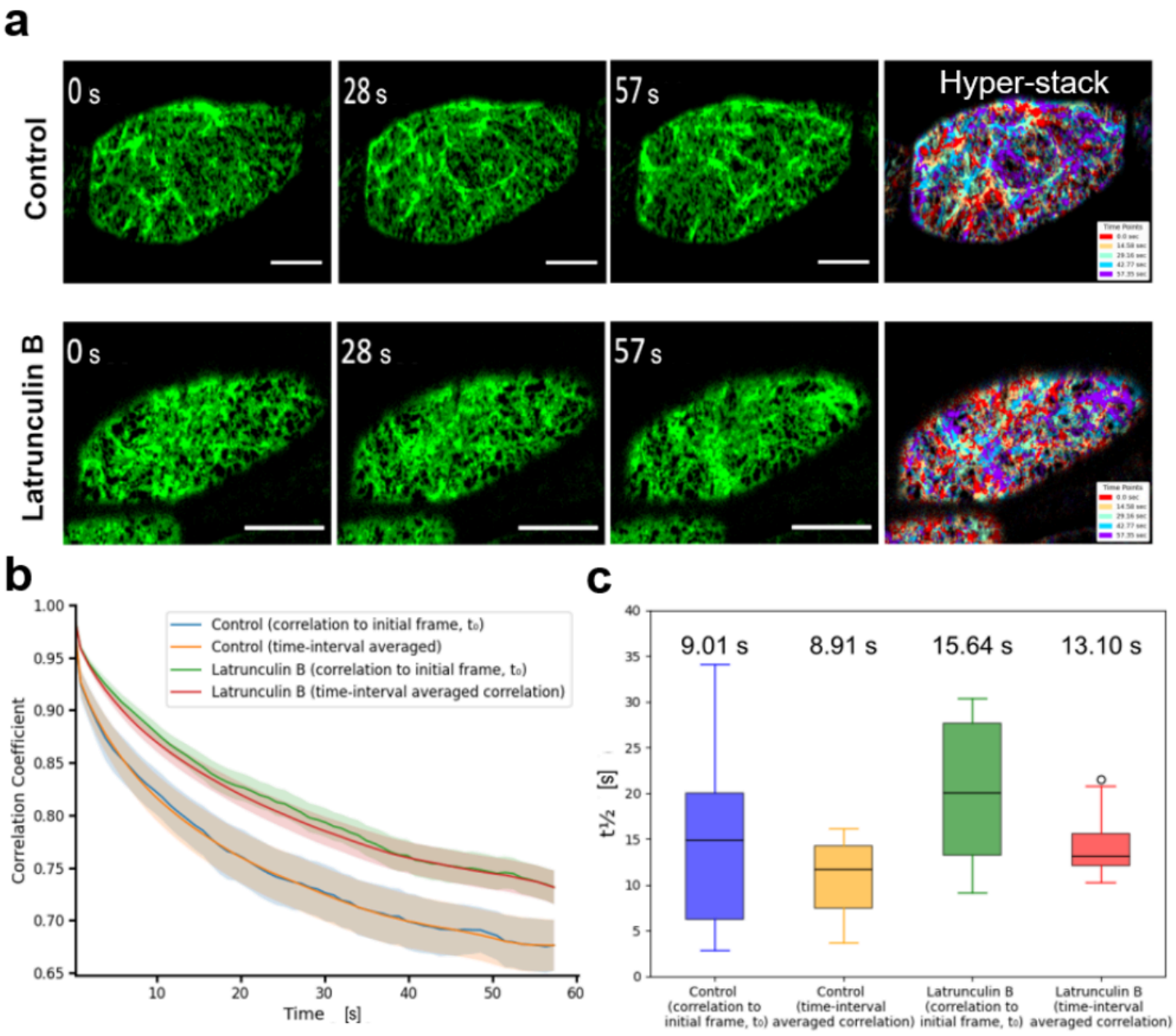

Figure 3

Analysis of the endoplasmic reticulum (ER) dynamics using correlation to the initial frame method and time-interval average correlation comparatively. (a) The dynamic behaviour of ER in *HDEL-GFP*transgenic plants were used to examine whether the two methods provide similar outcomes in control and Latrunculin B treated plants (treatment with 10 nM for 10 min before observation). Representative

images of equally spaced time intervals are presented. From each sample a color-coded hyper-stack of these frames was produced using Cell-Corr. (b) Quantification of the ER dynamics using the correlation coefficient as a function of time (13 cells were analysed for each sample). Both methods described were used for each sample, although no statistical significance was found between them (p = 1.0 for each separate sample tested with Kruskal-Wallis test). (c) Calculation of t1/2 parameter from each individual ROI using the same fitting model as Cell-Corr for every sample group, compared with the values extracted by the software using the complete data frame (numbers above each boxplot). Scale bar: 20 μM.

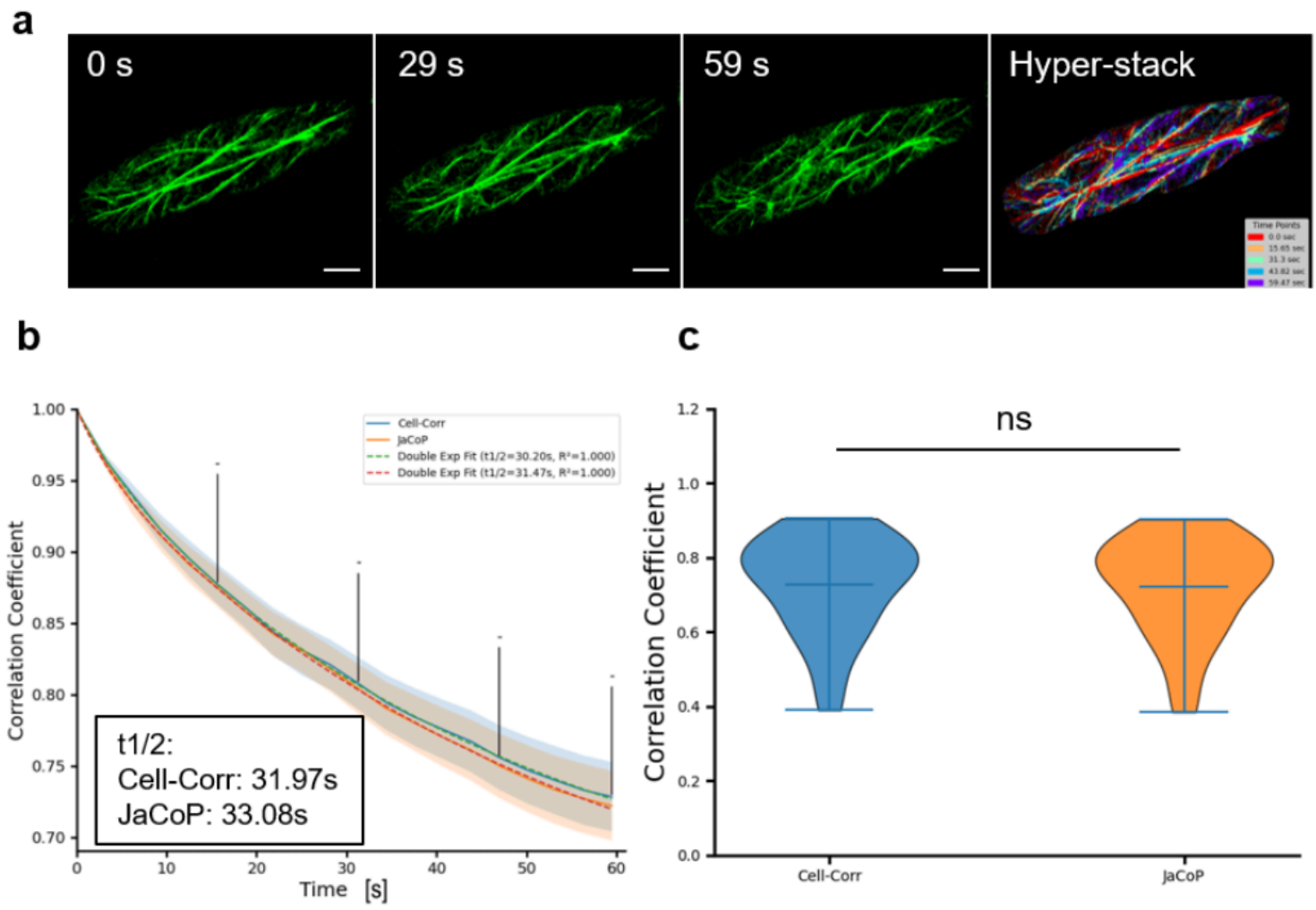

Figure 4

Comparison of PCCs between Cell-Corr and ImageJ plug-in JaCoP analysis. (a) Representative timeframes and color-coded hyper-stack of 4-day-old seedlings of hypocotyl epidermal cells of stable lines expressing *GFP-LifeAct*. (b) Quantification of actin dynamics with PCCs using Cell-Corr has no significant difference from the ones calculated with JaCoP (12.52s: p=0.85, 34.43s: p=0.862, 43.82s: p= 0.839 and 56.34s: p=0.931 as tested with Kruskal-Wallis). (c) Distribution of ROIs Correlation Coefficients among the initial and final frames as depicted in panel b. In total 30 cells were analyzed (from at least 10 seedlings). Not significant: ns. Scale bar: 20 μm.

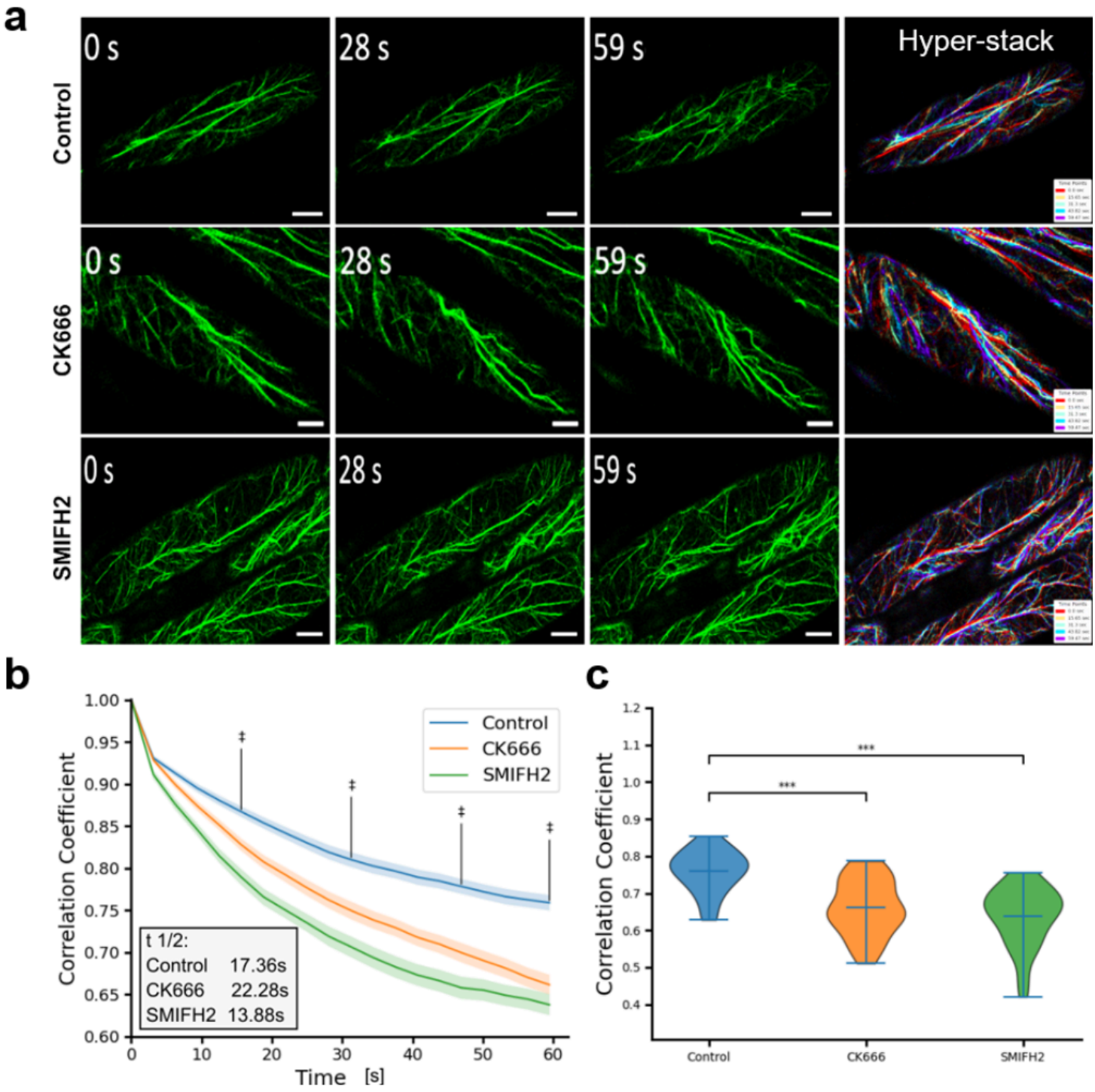

Figure 5

Impact of SMIFH2 and CK-666 inhibitors on the dynamics of F-Actin, analyzed with Cell-Corr. (a) hypocotyl epidermal cells of stable *GFP-LifeAct* line were used to quantify the dynamics of F-actin in control plants, 10 μM SMIFH2 treated for 4 days and 10 μM CK-666 treated plants for 10 min before observation. In the far-right column, merged images overlaying five equally spaced frames with different color each, is presented as a descriptive depiction of the changes in actin organization over time. (b) Quantification of the actin dynamics using the Correlation Coefficient between every frame and the initial

frame, expressed as a function of time. Statistical analysis was conducted using Kruskal-Wallis test (‡ corresponds to $p<0.05$). Estimated t1/2 values by Cell-Corr are given on the corresponding box. (c) Distribution of ROIs Correlation Coefficients among the initial and final frames as presented in panel b. Statistical significance was calculated with Kruskal-Wallis test (***: $p< 0.001$). Scale bar: 20 μm.

Supplementary Files

This is a list of supplementary files associated with this preprint. Click to download.

- Supplementarymaterial1.docx
- Movie6.mp4
- Movie4.mp4
- Movie3.mp4
- Movie5.mp4
- Movie1.mp4
- Movie2.mp4